LASER INDUCED DAMAGE TO MIRRORS AT TWO PULSE DURATIONS

E. S. Bliss, et al

Air Force Cambridge Research Laboratories

Prepared for:

Advanced Research Projects Agency

25 July 1972

AFCRL-72-0423
25 JULY 1972
PHYSICAL SCIENCES RESEARCH PAPERS, NO. 504

AIR FORCE CAMBRIDGE RESEARCH LABORATORIES
L. G. HANSCOM FIELD, BEDFORD, MASSACHUSETTS

Laser Induced Damage to Mirrors at Two Pulse Durations

Technical Report No. 2
Period 31 December 1971 to 30 June 1972

E.S. BLISS, CAPT, USAF
D. MILAM
R.A. BRADBURY

Details of illustrations in this document may be better studied on microfiche

Approved for public release; distribution unlimited.

AIR FORCE SYSTEMS COMMAND
United States Air Force

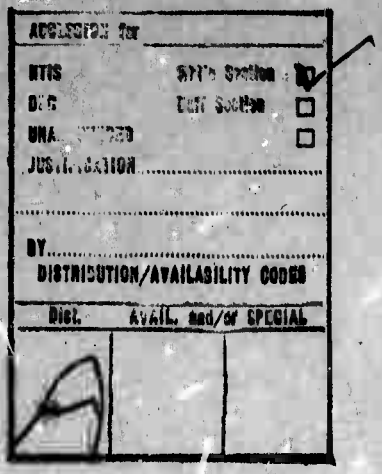

Qualified requestors may obtain additional copies from the Defense Documentation Center. All others should apply to the National Technical Information Service.

Unclassified
Security Classification

DOCUMENT CONTROL DATA - R&D

(Security classification of title, body of abstract and indexing annotation must be entered when the overall report is classified)

1. ORIGINATING ACTIVITY *(Corporate author)*
Air Force Cambridge Research Laboratories (OPL)
L. G. Hanscom Field
Bedford, Massachusetts 01730

2a. REPORT SECURITY CLASSIFICATION
Unclassified

2b. GROUP

3. REPORT TITLE
LASER INDUCED DAMAGE TO MIRRORS AT TWO PULSE DURATIONS
TECHNICAL REPORT NO. 2—PERIOD 31 DECEMBER 1971 TO 30 JUNE 1972

4. DESCRIPTIVE NOTES *(Type of report and inclusive dates)*
Scientific. Interim.

5. AUTHOR(S) *(First name, middle initial, last name)*
E. S. Bliss, Capt. USAF
D. Milam
R. A. Bradbury

6. REPORT DATE
25 July 1972

7a. TOTAL NO. OF PAGES
36

7b. NO. OF REFS
9

8a. CONTRACT OR GRANT NO.
ARPA 14

b. PROJECT, TASK, WORK UNIT NOS. 6100-01-01

c. DOD ELEMENT 61101D

d. DOD SUB ELEMENT

9a. ORIGINATOR'S REPORT NUMBER(S)
AFCRL-72-0423

9b. OTHER REPORT NO(S) *(Any other numbers that may be assigned this report)*
PSRP, No. 504

10. DISTRIBUTION STATEMENT
Approved for public release; distribution unlimited

11. SUPPLEMENTARY NOTES
Sponsored by Advanced Research Projects Agency, ARPA Order No. 1434

12. SPONSORING MILITARY ACTIVITY
Air Force Cambridge Research Laboratories (OPL)
L. G. Hanscom Field
Bedford, Massachusetts 01730

13. ABSTRACT

The damage thresholds of eight, multiple layer dielectric, 95 percent reflecting mirrors have been measured for single pulses of 20 nsec and 20 psec duration. In both sets of measurements the pulse energy, an oscilloscope trace of the pulse, and the beam's transverse energy density profile at the surface being damaged are recorded for each shot. The variation of the threshold from mirror to mirror and as a function of pulse duration, beam radius, and appearance under microscopic examination is discussed in the context of possible damage mechanisms.

DD FORM 1 NOV 65 1473

Unclassified
Security Classification

14. KEY WORDS	LINK A		LINK B		LINK C	
	ROLE	WT	ROLE	WT	ROLE	WT
Laser induced damage						
Dielectric mirrors						
Mode-locked ruby laser						
TEM_{00}-mode						
Q-switched ruby laser						

AFCRL-72-0423
25 JULY 1972
PHYSICAL SCIENCES RESEARCH PAPERS, NO. 504

OPTICAL PHYSICS LABORATORY PROJECT 6100

AIR FORCE CAMBRIDGE RESEARCH LABORATORIES

L. G. HANSCOM FIELD, BEDFORD, MASSACHUSETTS

Laser Induced Damage to Mirrors at Two Pulse Durations

Technical Report No. 2

Period 31 December 1971 to 30 June 1972

E.S. BLISS, CAPT, USAF
D. MILAM
R.A. BRADBURY

Spor sored by
Advonced Reseorch Projects Agency
ARPA Order No. 1434

AIR FORCE SYSTEMS COMMAND
United States Air Force

Abstract

The damage thresholds of eight, multiple layer dielectric, 95 percent reflecting mirrors have been measured for single pulses of 20 nsec and 20 psec duration. In both sets of measurements the pulse energy, an oscilloscope trace of the pulse, and the beam's transverse energy density profile at the surface being damaged are recorded for each shot. The variation of the threshold from mirror to mirror and as a function of pulse duration, beam radius, and appearance under microscopic examination is discussed in the context of possible damage mechanisms.

Contents

Illustrations

Tables

Technical Report Summary

Purpose of Project

The purpose of this research is to gain an understanding of the processes by which laser radiation causes damage to nominally transparent materials, especially those used in the laser themselves.

Equipment Development

This project began against a background of confusing and contradictory information concerning laser induced damage to transparent dielectrics. Experimental results of different workers were difficult, often impossible, to compare, and the connection between theoretical and experimental results was tenuous at best. Having concluded that lack of appreciation for the complexity of the problem had led to inadequate experimental control and monitoring in earlier work, we undertook the task of designing, building, and testing a ruby laser damage test facility capable of obtaining experimental data under carefully controlled and fully monitored conditions. A detailed description of this facility was given in a previous report (Tech. Report No. 1). The present report describes the first experiments conducted with the facility.

Conclusions

Measurements with fully monitored and properly controlled laser damage systems yield useful data concerning the damage properties of laser system components.

Laser Induced Damage to Mirrors at Two Pulse Durations*

Technical Report No. 2
Period 31 December 1971 to 30 June 1972

I. INTRODUCTION

For several years an effort has been underway at the Air Force Cambridge Research Laboratories to perfect a mode-locked ruby laser system capable of reliably producing single subnanosecond pulses with a smooth and radially symmetric energy density profile and enough energy to damage dielectric materials with spot sizes larger than 0.1 mm. Such a system is now in use and is described in detail in earlier publications (Bliss and Milam, 1972; Milam, 1971). To complement the mode-locked system and to facilitate experimental identification of the laser-induced-damage mechanisms by determination of their pulse duration dependence (Bliss, 1970), a standard Q-switched ruby laser system has also been constructed which meets the same reliability, radial energy distribution, and total energy requirements and operates in a single longitudinal mode as well. Figure 1 contains block diagrams of both systems. This report describes laser induced damage measurements performed on nine commercially produced dielectric mirrors using these two lasers.

(Received for publication 25 July 1972)

* This research was supported jointly by the Air Force and the Advanced Research Projects Agency of the Department of Defense.

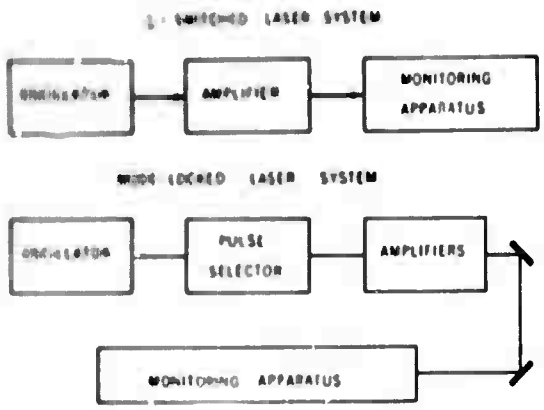

Figure 1. Block Diagrams of the Laser Systems

2. LASER DAMAGE MONITORING APPARATUS

Meaningful laser-induced-damage experiments demand precise characterization of the laser pulse causing the damage. Accordingly, each pulse is scrutinized in unprecedented detail.

2.1 Q-Switched System Monitoring

Figure 2 is a schematic diagram of the monitoring apparatus for experiments using Q-switched pulses. The beam enters from the left and passes through two beam splitters. The first one deflects a portion of the beam to a fast diode which drives a Tektronix 454 oscilloscope and provides a filmed record of the temporal

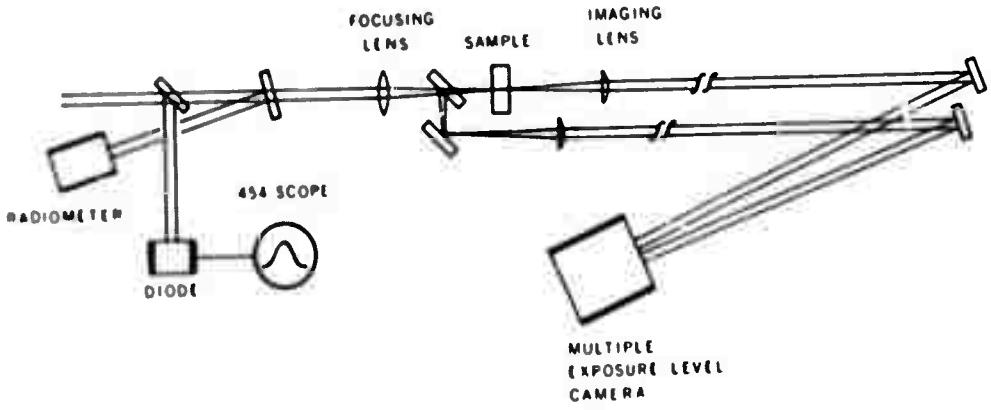

Figure 2. Monitoring Apparatus for Damage Experiments with Q-Switched Pulses

development of each pulse. The second beam splitter directs a known fraction of the beam to an EG&G radiometer, which is used to determine the energy of each pulse.

The beam then passes through a 50-cm focal-length lens and, except for a small portion, is focused onto the damage sample. When the test sample is a high reflectivity mirror, the path shown beyond the sample is not used, and the mirror is tipped very slightly to avoid direct reflections back to the amplifier. The small reference beam, which is split off after the focusing lens, is identical to the damaging beam except for its energy content and it can be utilized for monitoring the focused radial energy distribution as follows: A calibrated reticle is inserted in the reference beam in the plane corresponding to the mirror surface in the main beam. An imaging lens is then placed such that the reticle is imaged onto the film in the multiple-exposure level camera (Burnham, 1970). For ruby lasers Polaroid film Type 55 is ideal since it provides a positive for visual examination and a negative for densitometer analysis. The magnification of the imaging system is determined by photographing the reticle with 0.69 μm light. Then the reticle is removed and the camera now records the radial energy density profile of each pulse in the damage plane. Examples of such photographs will be discussed in Section 3.1.2.

2.2 Mode-Locked System Monitoring

Figure 3 is a schematic diagram of the monitoring apparatus for experiments using mode-locked pulses (Bliss and Milam, 1972). The principal features are the same as for the Q-switch pulse monitoring system, but there are some differences. The focusing is done by a lens pair whose effective focal length can be varied by changing the lens spacing (an effective focal length of approximately 1 m was used for all the measurements reported in this paper). Both an EG&G radiometer and a Quantronix 500/504 calorimeter/energy-meter are used for energy measurement. Although the calorimeter is blocked when a high reflectivity

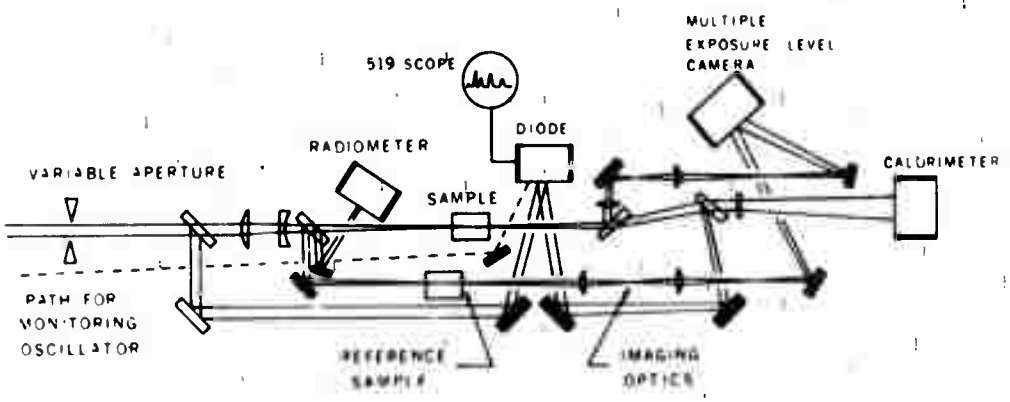

Figure 3. Monitoring Apparatus for Damage Experiments with Subnanosecond Pulses

mirror is used for a sample, it is used as an occasional check on the radiometer by removing the sample.

The fast diode drives a Tektronix 519 oscilloscope and examines light arriving along several paths simultaneously. A small portion of the oscillator output is picked off at the pulse selector (Bliss and Milam, 1972) and enters the diode along the dotted path in Figure 3. One percent of the amplified selected pulse is split off just ahead of the focusing optics and directed onto the diode with a delay appropriate to display it between pulses in the oscillator's mode-locked train. The remaining path to the diode is for monitoring the pulse after passage through a transparent damage sample and is not used for mirror studies.

The radial energy distribution in the damage plane is imaged into the multiple exposure camera by a lens pair instead of single lens. This allows the first lens to be well removed from the sample area and gives more flexibility for imaging different planes and changing magnification. As in the Q-switched monitoring system the energy density profile in the main beam is not monitored for mirror damage experiments and so no reference sample is required.

3. OUTPUT PROPERTIES OF THE LASERS

3.1 Q-Switched System

3.1.1 TEMPORAL PROFILE

It is known that smooth, apparently single longitudinal mode oscilloscope traces obtained by spacially integrating over the whole beam on a diode do not guarantee that the temporal development of the pulse is the same over the whole beam (DeShazer and Parks, 1971). In order to determine whether deviations from ideal temporal behavior off the beam axis might be related to deviations from the ideal radial energy distribution, a sequence of shots was fired in which the output mirror of the Q-switched oscillator was rotated by 4 sec of arc about the vertical axis after each shot. After appropriate attenuation the oscillator output was directed into the multiple exposure-level camera without focusing, and each shot was photographed in turn. Figure 4a shows the results.

Each shot produces a vertical row of successively less exposed energy density profiles, and the shots on the left show a slightly elongated pattern with the top tipped to the right, while the shots on the right show a similar elongation with a tip to the left. When the temporal profile is examined through a pinhole on axis (Figure 4b, right) and through a vertically displaced pinhole (Figure 4b, left) for the mirror position giving no detectable tip (5th from the right), the off-axis temporal profile is found to be considerably different from that on axis. If the process is now repeated for mirror rotations about the horizontal axis, however,

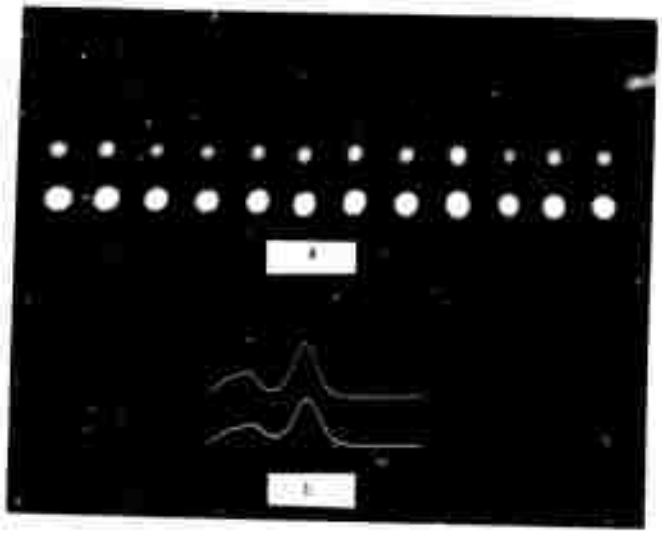

Figure 4. (a) Multiple Exposure-Level Photographs of the Oscillator Output for a Range of Mirror Rotations About the Vertical Axis. The output mirror was rotated by 4 sec of arc between successive exposures. (b) Temporal profile detected through a pinhole on axis (right) and through a vertical displaced pinhole (left) for the shot producing the fifth exposure from the right in (a)

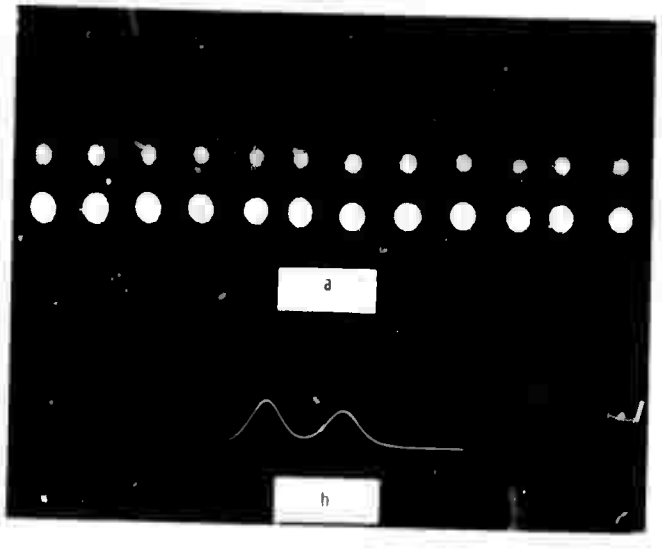

Figure 5. (a) Multiple Exposure-Level Photographs of the Oscillator Output for a Range of Mirror Rotations About the Horizontal Axis. The output mirror was rotated by 4 sec of arc between successive exposures. (b) Temporal profile detected through a pinhole on axis (right) and a vertically displaced pinhole (left) for the shot producing the far right exposure in (a)

with 4-sec rotations being made until the spot is no longer elongated but round as for the far right mirror position of Figure 5a, then the same temporal profile is found at both pinholes.

We conclude that a genuinely round output from the Q-switched oscillator implies uniform temporal behavior over the whole beam. Typically the preparations for a series of damage tests included an examination of the oscillator output, but it was not always done with the thoroughness demonstrated in Figures 4 and 5. Consequently, it is quite possible that some of the measurements to be described in Sections 4 and 5 were performed with pulses whose off-axis temporal behavior was less than ideal. The effect of small temporal deviations off-axis on the results of our damage tests is assumed to be negligible.

In Figure 6 the spacially integrated temporal pulse profile, as recorded by the monitoring apparatus in Figure 2, has been compared for three randomly selected pulses out of a series of some 220 shots. Pulse No. 217 is indicated by a solid curve and points, measured from the scope traces of shots 11 (O) and 89 (□), are plotted on a normalized scale which forces the pulses to coincide at their peak power points. The fact that all three pulses fall on essentially the same curve demonstrates the high degree of repeatability obtained in the temporal shape of the pulse.

3.1.2 SPACIAL PROFILE

Figure 7a shows two examples of the Q-switched pulse's radial energy distribution in the damage plane as photographed by the imaging system described in Section 2.1. Each pulse produces a horizontal line of spots in which adjacent exposures differ by a factor of two. The microdensitometer traces of three consecutive shots shown in Figure 7b verify the impression, gained by visual examination of the photographs, that the energy density varies smoothly with radius. Furthermore, we have determined by constructing energy density radius curves from the densitometer traces (Winer, 1966) that the radial dependence of the energy distribution is Gaussian.

3.2 Mode-Locked System

3.2.1 TEMPORAL CHARACTERISTICS

The mode-locked oscillator produces a train of short pulses separated by approximately 7 nsec, from which a single pulse is selected for amplification. In Figure 8 oscilloscope traces of four consecutive shots show the mode-locked train with the selected pulse missing and the amplified selected pulse displayed between the first two recorded pulses of the train. The extra little bump appearing just before the amplifier pulse in the bottom three traces is a stray reflection onto the diode and may be ignored.

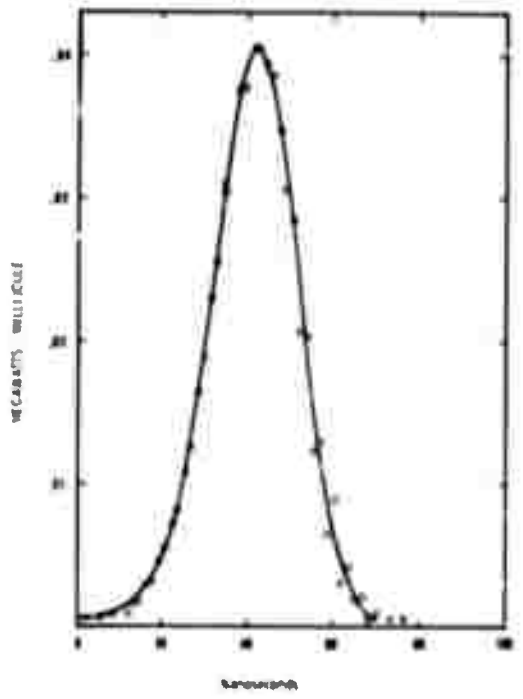

Figure 6. Spacially Integrated Temporal Profile of Three Q-Switched Pulses from a Series of 220 Shots: (O) Shot 11, (□) Shot 89, (—) Shot 217

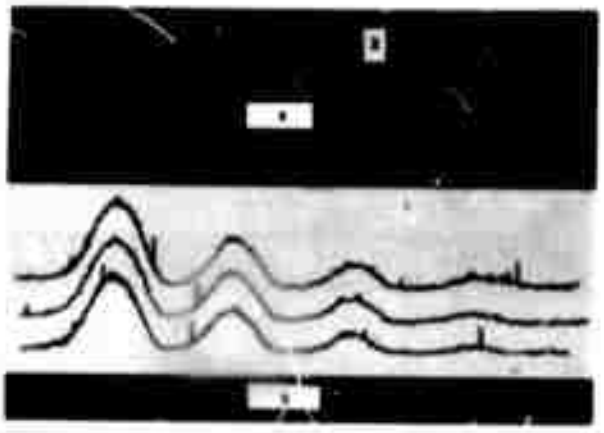

Figure 7. (a) Multiple Exposure-Level Photographs Showing the Radial Energy Distribution in the Damage Plane for Two Q-Switched Pulses. The dimension of the scale marker is 100 μm. (b) Microdensitometer traces of multiple exposure-level photographs for three consecutive Q-switched pulses. Adjacent exposures on each trace differ by a factor of two

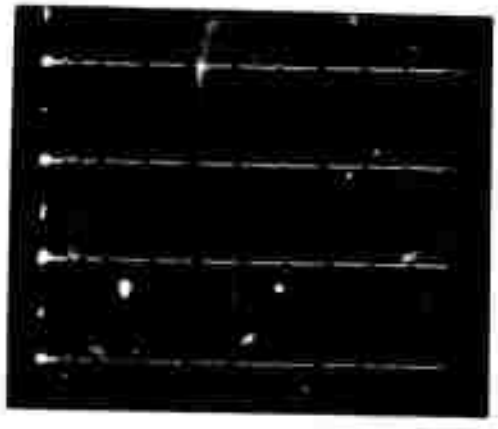

Figure 8. Oscilloscope Traces for Four Consecutive Firings of the Mode-Locked Ruby Laser. The selected pulse is missing from the train just to the right of the center, and after amplification it is displayed between two early pulses of the train at the left

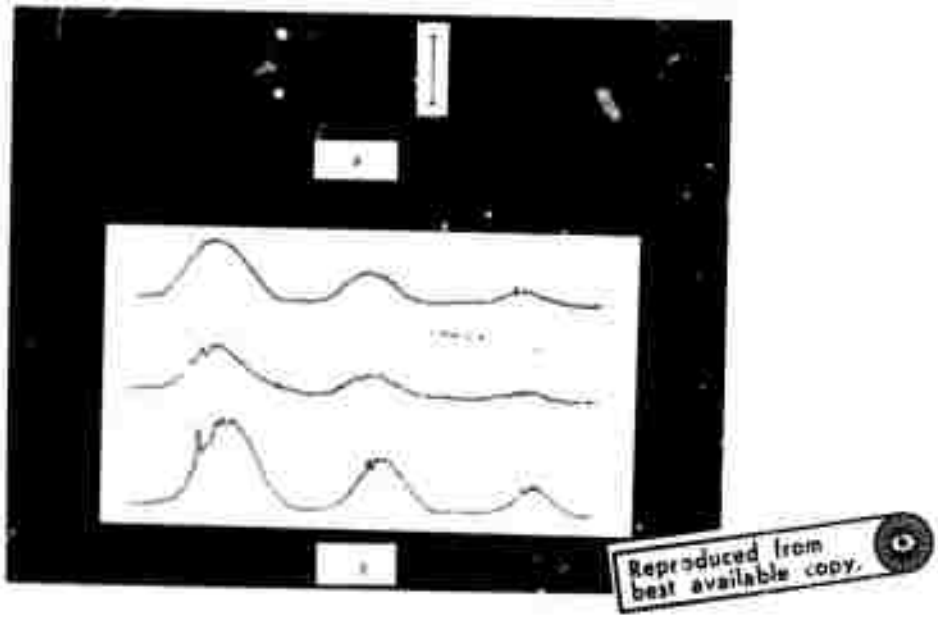

Figure 9. (a) Multiple Exposure-Level Photographs Showing the Radial Energy Distribution in the Damage Plane for Three 20-psec Pulses. The dimension of the scale marker is 1 mm. (b) Microdensitometer traces of multiple exposure-level photographs for three consecutive 20-psec pulses. Adjacent exposures on each trace differ by a factor of 1.85

The duration of the mode-locked pulses generated by the oscillator has been estimated from time-integrated two-photon fluorescence photographs to be approximately 20 psec. To check for the possibility that the pulse duration changes during amplification or that pulses from different parts of the pulse train have different durations, two-photon measurements of single amplifier pulses are planned, but have not yet been accomplished. Even without such measurements, however, it is known from the impulse response of the diode-oscilloscope combination that the pulse duration of the amplified pulses is less than 100 psec. For the case of pulses selected from properly locked trains, the amplified pulse always gives the same impulse shape scope response as the oscillator output.

3.2.2 SPACIAL PROFILE

The examples of focused radial energy density profiles for single mode-locked pulses shown in Figure 9 are similar to those shown for Q-switched pulses in Figure 7. Since the pronounced spike appearing on the left side of the first exposure in the bottom trace does not appear in the adjacent exposure, it is not an intensity spike in the beam and must be identified as a spot or a scratch on the film. Construction of energy density radius curves from these densitometer traces reveals some small departures from a true Gaussian profile. The errors in damage threshold resulting from treating the profile as Gaussian are small, however, compared with the uncertainty already existing in total energy measurement.

4. MIRROR DAMAGE EXPERIMENTS

Using the lasers and monitoring techniques described above, experiments have been conducted on nine mirrors from five manufacturers. Basic information about the mirrors is given in Table 1.

Table 1. Mirrors Used for Damage Tests

Designation	Coating Composition	No. of Layers	Reflectivity (%)	Density of Scattering Centers
A-1	TiO_2/SiO_2	9	94.3	Moderate
A-4	TiO_2/SiO_2	7	92.5	Low
A-6	TiO_2/SiO_2	7	92.5	Low
C-1	TiO_2/SiO_2	9	94.3	Low
D-1	TiO_2/SiO_2	18	96.8	Low
C-4	ZrO_2/SiO_2	13	95.6	High
C-7	ZrO_2/SiO_2	13	96.0	Low
E-1	ZrO_2/SiO_2	25	95.7	High
B-1	ZnS/ThF	21	96.2	Moderate

4.1 Observable Features of the Damage Sites

When viewed under an optical microscope at a magnification of thirty, the most frequently observed form of damage has the appearance of one or more bright rings having the same shape as the beam's radial energy density profile. Sometimes one or more randomly located bright spots are observed within this overall pattern. Examination of such sites in a scanning electron microscope reveals considerably more detail. In Figures 10 and 11 the ring appearance is seen to be caused by a step inside of which one or more of the quarter-wave layers have been removed. Since the sample is viewed from an angle in a scanning electron microscope, the round damage site appears to be compressed along the vertical axis. Figure 12 is a close-up view of the bright spot seen below and to the left of center in Figure 10. Since the position of this spot does not correspond to the position of maximum intensity in the beam, it is probably the result of a local absorbing center or other small scale mirror defect.

The photographs just described show damage sites caused by Q-switched pulses, but the physical characteristics of sites damaged by single mode-locked pulses are similar. In Figures 13, 14, and 15, for example, the same overall pattern of well-defined rings with a randomly located little crater is observed. In Figures 16 and 17 a tendency toward smaller damage sites and removal of fewer layers is observed for less energetic pulses. Figure 16 also illustrates the fact that the transition from one layer to the next is not always a well-defined step. Since the energy density profile of this pulse in the plane of the mirror is observed to be a smooth function of radius on the multiple exposure-level photograph taken during the experiment, the irregular pattern of material removal in the central region of this site suggests a degree of inhomogeneity in the coating itself.

In contrast to the damage site characteristics described above, the affected areas on some mirrors appear under the optical microscope to be made up of a large number of closely packed scattering sites. Two examples of this type of damage are given in the lower right portion of Figure 18. This mirror (E-1) has a generally high density of scattering centers even in areas not exposed to laser radiation, but it is not yet established whether they contribute to the characteristics of the damage sites themselves. The sites just described are produced by 20-psec pulses and the ring type sites on the same mirror in the upper half of the figure are produced by 20- nsec pulses. For mirror B-1 just the opposite is found: 20 psec pulses produce rings and 20-nsec pulses produce scattering centers.

Figure 10. Scanning Electron Microscope (SEM) Photograph of a Damage Site Produced by a Q-Switched Pulse. The site dimension is 250 μm from left to right

Figure 11. SEM Photograph of the Edge of a Damage Site. The entire photo is 57 μm wide

Figure 12. SEM Photograph of the Bright Spot Seen Below and to the Left of Center in Figure 10. The width of the photo is 11 μm

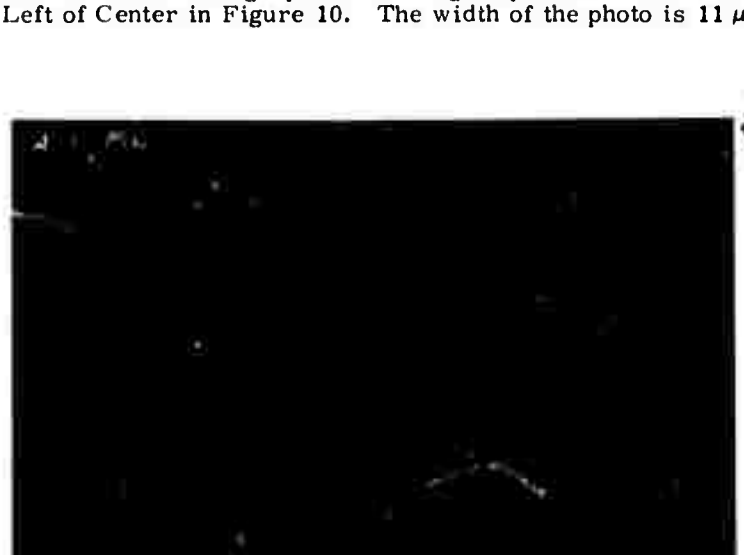

Figure 13. SEM Photograph of a Damage Site Produced by a 20-psec Pulse. The width of the photo is 436 μm

Figure 14. SEM Photograph of the Steps Seen in Figure 13. The width of the photo is 180 μm

Figure 15. SEM Photograph of the Bright Spot to the Right of Center in Figure 13. The width of the photo is 18 μm

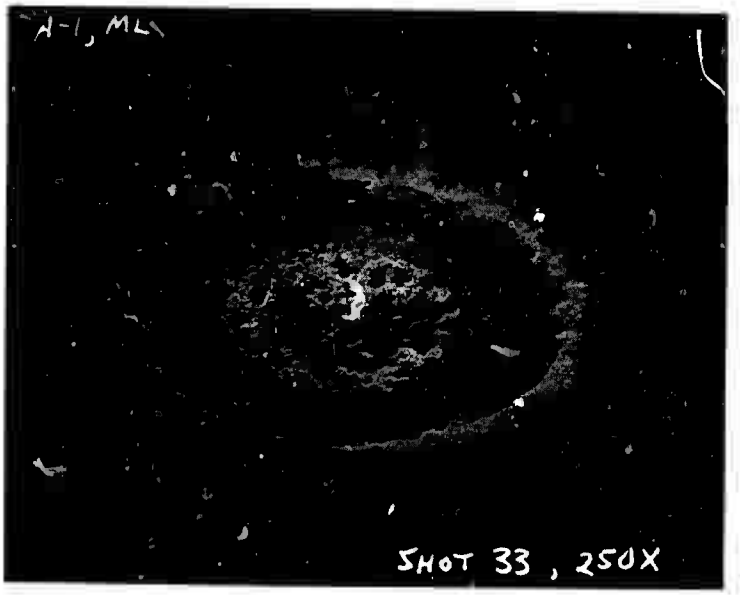

Figure 16. SEM Photograph of a Site Damaged by a Less Energetic 20-psec Pulse. An irregular pattern of material removal is evident in the central portion. The width of the photo is 456 μm

Figure 17. SEM Photograph of a Damage Site Produced by a 20-psec Pulse Having an Energy Density only Slightly Above Threshold. The width of the photo is 98 μm

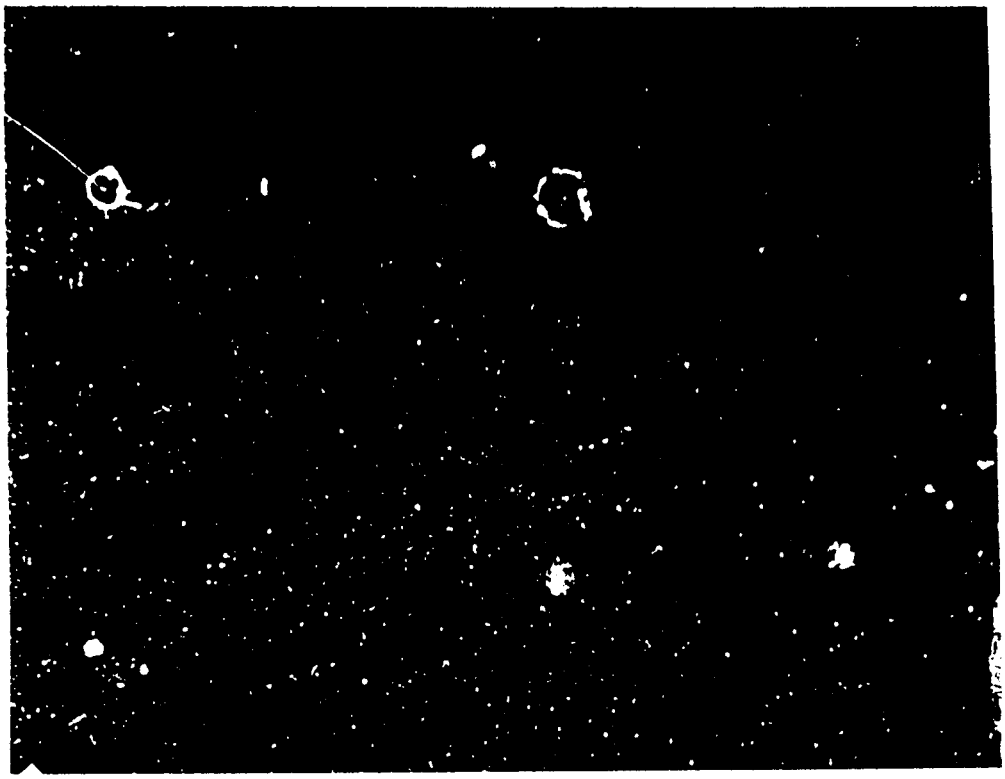

Figure 18. Optical Microscope Photograph of Scattering Site Type of Damage (lower row) Caused by 20-psec Pulse on Mirror E-1, for Which Q-Switched Pulses Produced Mostly Ring Type Damage (upper row). The spacing between the two sites in the right side of the lower row is 1 mm

1.2 Fogging Effects

Even when examination under the optical microscope reveals no obvious damage on a mirror, fogging the coating with one's breath often reveals clear evidence that the radiation has alter d the surface in some way. The microscope photos (a) and (b) in Figure 19 illu .ate this point. A striking feature of this effect is that an area much larger than the otherwise detectable damage region is affected. In (c) and (d) of Figure 19, for example, a region many times larger than the beam itself has different fogging properties. To some extent the effect is temporary as evidenced by the difference in appearance of the 20-hour old sites and the 1-hour old sites.

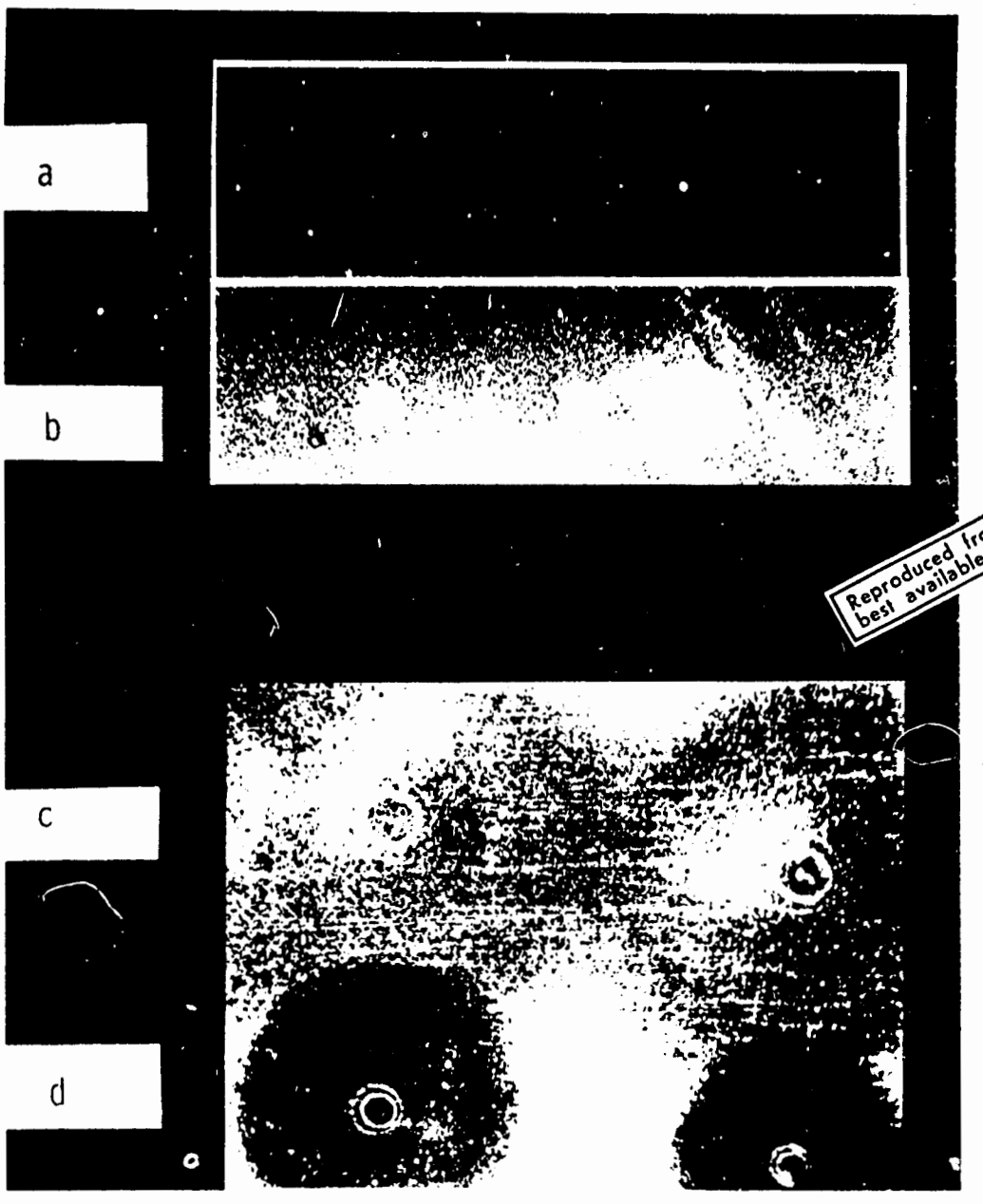

Figure 19. Optical Microscope Photographs of (a) a Damaged Unfogged Mirror, (b) the Same Mirror After Fogging with Breath, (c) and (d) Higher Magnification View of Some Sites Which Were Damaged Twenty Hours Before the Fogged Photograph and One Hour Before the Photograph Respectively

4.3 Data Reduction

For each set of Q-switched damage measurements randomly selected pulses are quantitatively checked to verify the Gaussian radial dependence of the energy density and the reproducibility of the temporal pulse shape. These two important properties are also checked qualitatively for each shot by visual examination of the monitoring photographs. Any shots showing irregularities of either temporal or spacial profile are rejected. The Gaussian radius is measured for each remaining shot and combined with the pulse energy measurement to give a value of energy density on axis for each pulse. As will be shown, the diameter of each damage site is also of interest, and it is measured from optical microscope photographs of the damaged coatings.

Data reduction for the mode-locked pulse experiments, particularly the determination of pulse energy, is not quite so straightforward. Complications arise because of the limitations placed on energy measuring devices at this pulse duration. The calorimeter, for example, reads 100 mJ full scale on the most sensitive scale and its thermal sensitivity of 3J/°C makes compensation for ambient temperature changes very difficult. This leads to background variations which in the worst cases are on the order of the several millijoule pulse energies being measured. The radiometer, which monitors a small fraction of the pulse energy on each shot, must also be used on its most sensitive scale (0.35 mJ full scale) where background noise is a problem. The seemingly expedient solution of putting a larger percentage of the laser output into the radiometer is risky since at such short pulse durations very little energy is required to cause saturation effects in the photodiode, invalidating its calibration.

To circumvent these difficulties a series of shots is fired with no sample in place so that simultaneous calorimeter and radiometer readings as well as 519 scope traces are obtained. In a plot of calorimeter readings vs radiometer readings, the noise in both energy detectors scatters the points about a best straight line relating the absolute calibration of the two devices. It is found that the radiometer predicts 1.18 times the energy arriving at the sample location as that predicted by the calorimeter. Since neither measurement is known to be intrinsically more accurate than the other, the average of 0.924 times the radiometer reading is taken as the energy of a given pulse. Plotting the radiometer reading vs the height of the amplified pulse in the 519 scope trace provides a similar calibration curve of pulse energy vs 519 pulse height. The noise on the scope trace is typically much less than the noise on the radiometer; so the pulse height on the 519 scope makes a more consistent indicator of amplified pulse energy and when calibrated as described above, it is used as the primary energy measuring instrument. Radiometer readings are still taken throughout the run, however, to provide a constant check on the calibration curve.

An obvious difference between the Q-switched and mode-locked damage measurements is that no detailed analysis can be made of the temporal profile of the 20-psec pulse. Any pulses longer than about 100 psec can be rejected on the basis of the 519 trace, however, as can shots giving a double pulse or a poorly locked train.

4.4 Variation of Damage Site Diameter with Energy Density

A convenient way to display the mirror damage data is on a plot of damage site diameter vs the pulse energy density on axis. Figure 20 shows such a plot for the Q-switch pulse damage tests on mirror A-4. For low enough energy densities no evidence of damage is found (O). For energy densities above 30 or 35 J/cm^2 some randomly located small scattering centers are created, but there is no well-defined pattern to which a diameter can be assigned (Δ). Finally, for energy densities above about 45 J/cm^2 well-defined damage sites develop with diameters that are larger for more energetic pulses.

From such data two kinds of thresholds can be defined, the "practical damage threshold" below which no damage is caused by a single shot and a higher idealized threshold, a "perfect coating threshold", below which damage seems to be associated with local flaws of some sort rather than with inherent coating limitations. In Figure 20 the curve through the data is drawn to intersect the density axis at a point corresponding to the practical threshold. A curve drawn through the perfect coating threshold would intersect the axis at about 45 J/cm^2 and rise more steeply to pass through the remaining data points.

The simplest assumption, which predicts an increase of site diameter with energy density on axis, is that a coating damages only out to the radius at which the energy density drops below some critical value. The Gaussian energy distribution function can be solved for the diameter at which a given critical energy density is reached as a function of the on-axis energy density. The resulting curve is included in Figure 20 for a threshold value of 30 J/cm^2. This curve does pass through two of the measurable - site data points but falls well below the data at higher energies. A similar curve for a threshold of 45 J/cm^2 would completely miss the data.

Plots of measured site diameter vs Q-switched on-axis energy density for six of the nine mirrors are shown (without data points) in Figure 21. The curves are drawn to cross the axis at the practical damage threshold, and in general the perfect coating threshold is higher as seen in Table 2. All of these curves show damage sites that are larger at high energy than predicted by the simple constant-energy density assumption discussed above.

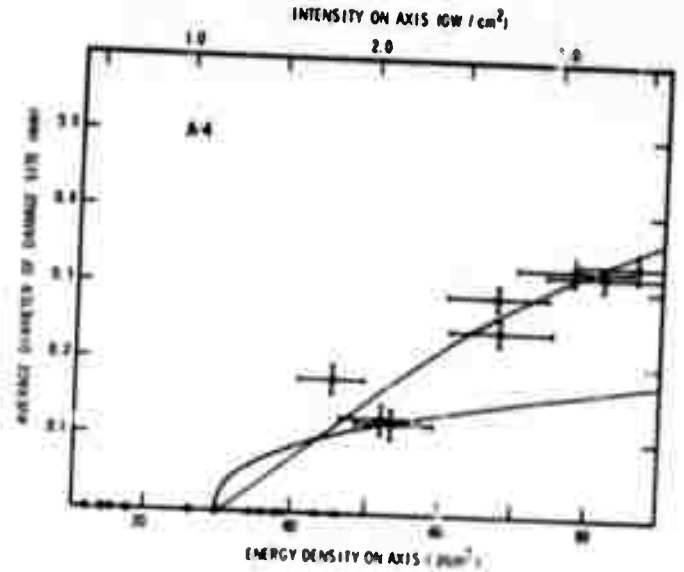

Figure 20. Damage Site Diameter vs Q-Switched Pulse Energy Density on Axis for Mirror A-4. Shots causing no detectable damage are indicated by (O), those causing only randomly located small scattering centers by (Δ), and sites with well-defined diameters by (O) at finite diameter values. A curve is drawn through the data points to intersect the axis at the practical damage threshold. The second curve gives the damage site diameter predicted on the assumption that any place on the coating will damage when subjected to an energy density of 30 J/cm^2

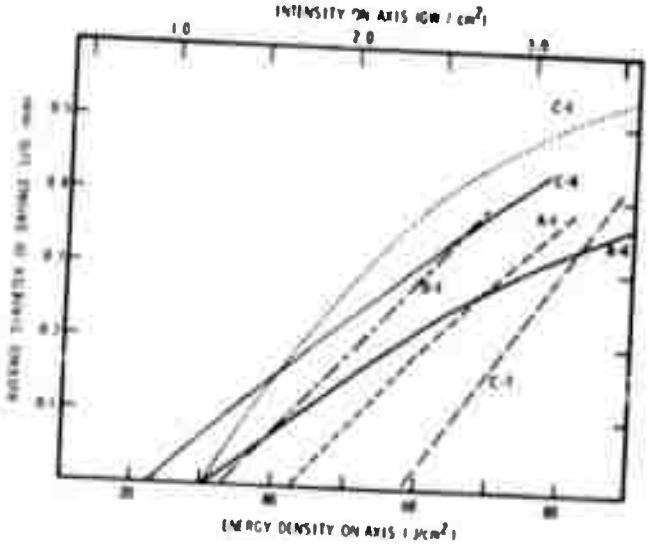

Figure 21. Damage Site Diameter vs Q-Switched Pulse Energy Density on Axis for Six Mirrors

Table 2. Measured Threshold Values

Mirror	Threshold at 20 psec[a]	Threshold at 23 nsec[b]	
		Practical	Perfect coating
	J/cm^2 on axis	J/cm^2 on axis	J/cm^2 on axis
A-1	1.6	43	46
A-4	2.2	30	46
A-6	-	-	26
C-1	1.8	30	30
D-1	1.6	33	38
C-4	1.9	23	31
C-7	1.8	58	60
E-1	2.9	47	47
B-1	0.6	16	24

(a) For the mode-locked pulse the beam diameter at half the on-axis energy density is 197 μm.

(b) For the Q-switched pulse the beam diameter at half the on-axis energy density is 130 μm.

Plotting the data from damage tests with single mode-locked pulses gives similar curves. There are some notable differences, however. First, all of the detected damage sites have measurable diameters, eliminating the distinction between the two threshold definitions discussed above. Second, a sharp rise in the curve immediately above threshold is clearly established by the data for most of the mirrors. Finally, for all but two of the mirrors, the damage sites are smaller at high energy than predicted by the constant energy density assumption. These differences are evident in Figure 22.

Plots of measured site diameter vs the on-axis energy density of the 20 psec pulse for seven of the mirrors are shown (without data points) in Figure 23. Mirrors B-1 and C-7 are exceptions in that they do fit a constant energy density curve quite well. Table 2 summarizes the results.

4.5 Dependence of Damage Threshold on Beam Diameter

To determine whether the observed damage threshold for 20-psec pulses measured with a 197-μm beam diameter can be meaningfully compared with the threshold for 23-nsec pulses measured with a 130-μm beam diameter, it is necessary to perform damage tests over a range of beam diameters at a fixed pulse duration. The results of such an investigation for mirror A-6 with 23-nsec pulses are shown in Figure 24. As in Figure 20 two kinds of thresholds are evident, at least for the large diameter beams, and so two curves are drawn,

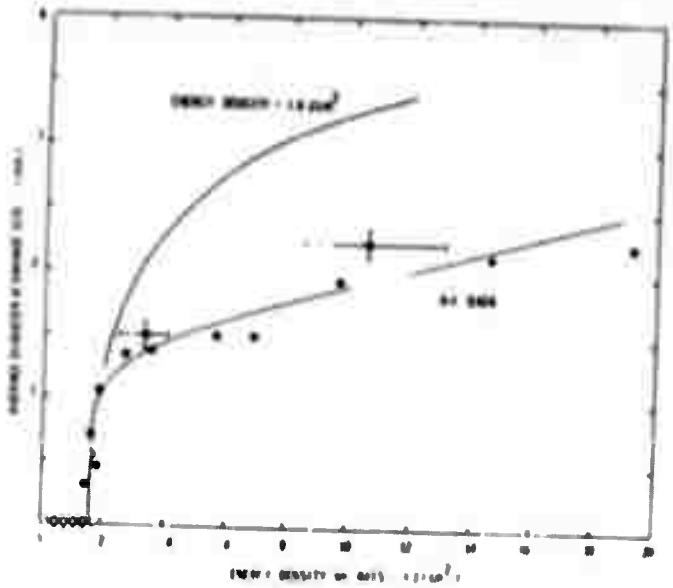

Figure 22. Damage Site Diameter vs 20-psec Pulse Energy Density on Axis for Mirror A-1. Shots causing no detectable damage are indicated by (X) and those causing damage by (●). The error bars shown are typical

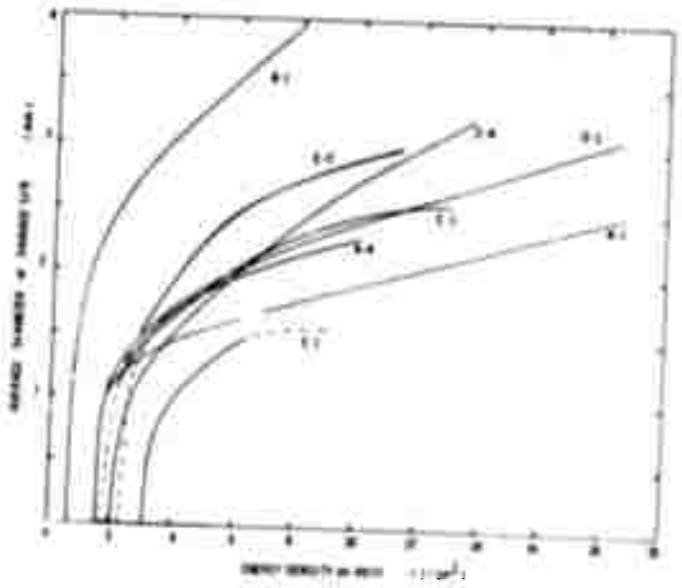

Figure 23. Damage Site Diameter vs 20-psec Pulse Energy on Axis for Seven Mirrors

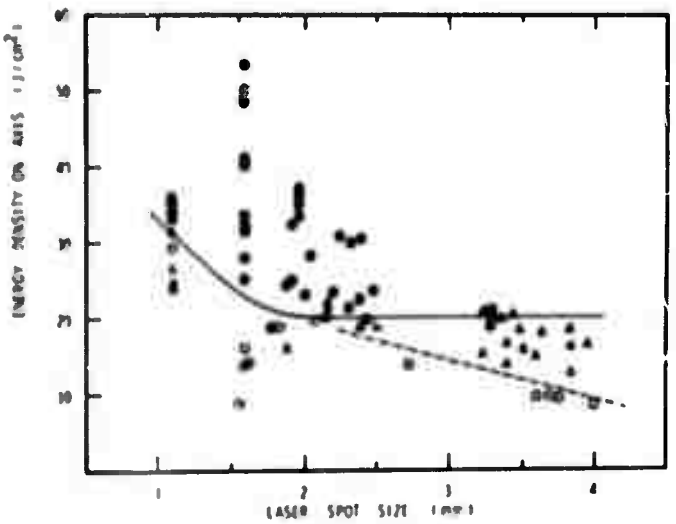

Figure 24. Q-Switched Damage Threshold vs the Beam Diameter at Half the On-Axis Energy Density for Mirror A-6. Shots causing no detectable damage are indicated by (O), those causing only randomly located small scattering centers by (Δ), and sites with well-defined diameters by (●). The solid curve indicates the best estimate for the variation of the perfect coating threshold, and the dashed curve the best estimate for the variation of the practical threshold

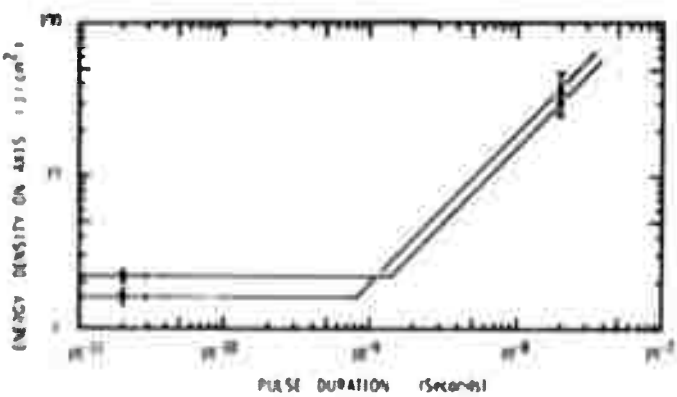

Figure 25. Single Pulse Damage Threshold vs Pulse Duration for Mirrors A-1 and A-4. The curves are drawn to fit the functional form suggested by theoretical considerations discussed in Section 5.4

the solid curve for the perfect coating threshold and the dashed curve for the practical threshold. These curves are simple fits to the data and do not represent any theoretically derived functional form. The decrease between 130 and 197 μm should be taken into account when comparing the mode-locked and Q-switched data.

4.6 Pulse Duration Dependence of Mirror Damage Thresholds

Even allowing for possible 25 percent reductions of the Q-switched damage thresholds in Table 2 if the measurements had been made with a 197-μm beam diameter as the 20-psec measurements were, the 23-nsec values are from ten to thirty times higher than the 20-psec energy density thresholds. Figure 25 illustrates this general observation with the results from mirrors A-1 and A-4. In this plot no adjustment for beam diameter dependence has been made since the size of such a correction could only be inferred from measurements on a different mirror. It is likely, however, that the Q-switched values should be recorded at a somewhat lower energy density. In this figure the functional form of the curves is suggested by theoretical considerations discussed in Section 5.4.

4.7 Accuracy and Reproducibility

4.7.1 EXPERIMENTAL ERRORS

For the Q-switched pulse data random errors in energy measurement and beam size determination can lead to uncertainties of plus or minus 10 percent in on-axis energy density measurements for single data points. As seen in Figure 20, however, either type of threshold can be determined to within about 5 percent for some of the mirrors.

For the mode-locked experiments, the uncertainties are somewhat larger because energy measurement is more difficult and there are small deviations from a true Gaussian energy density profile. Random errors in on-axis energy density for a single pulse may be as high as plus or minus 25 percent in this case. Again, however, threshold values are generally more accurately determined, as in Figure 22 where a reasonable estimate of uncertainty in threshold determination is plus or minus 10 percent.

In addition to the types of random error noted above, systematic error due to miscalibration of the energy measuring instruments must be expected. Readings from the calorimeter and radiometer, instruments which operate on entirely different physical principles, agree within 20 percent on the absolute value of the energy reaching the sample in the mode-locked experiments, suggesting that this error may be up to but probably does not exceed 20 percent for a given radiometer or calorimeter of the type used in this work.

4.7.2 MIRROR VARIATIONS

It is important to observe that ordering ten mirrors coated with specified dielectric materials from a particular manufacturer does not guarantee that ten identical mirrors will be delivered. The thresholds recorded in Table 2 for mirrors A-1, A-4, and A-6 and C-4 and C-7 illustrate the point. Decisions concerning the relative capabilities of several manufacturers should not be based on the performance of a single mirror.

5. POSSIBLE DAMAGE MECHANISMS

5.1 Uniform Linear Absorption

Sufficient linear absorption in a coating can heat the film to its melting point. However, the thermal time constants for conduction losses from the irradiated spot on the film, either radially or into the substrate, are expected to be long compared with both pulse durations. Thus, a uniform linear absorption model predicts the same energy density threshold over the whole pulse duration range and over the range of beam diameters tested as well. Neither prediction agrees with the experimental results An additional observation is that generally the damage looks more like cracking than melting. Of course, thermal expansion resulting from linear absorption heating can cause fractures too, but for this process the maximum induced stress occurs at 1.3 times the Gaussian beam diameter (the stress at radius r is proportional to the difference between the strain at r due to expansion of the material at smaller radii and the strain which would have occurred at r solely due to the local temperature increase (Hiliss, 1970)). The damage sites produced near the threshold energy density are consistently smaller than this.

5.2 Local Defects

There is no doubt that small scale local defects can account for some of the damage features reported here. Figures 12 and 14 are examples of pits believed to be caused by the explosion of small absorption centers. It is likely that for mirrors exhibiting a large difference between the practical damage threshold and the perfect coating threshold, small absorbing centers are causing the low level damage. Possible defects include dirt, incompletely oxidized coating material, or some other form of nonuniform deposition. The decrease of practical threshold with increasing beam diameter may be related to the increased likelihood of finding a defect with a large beam. For some mirrors, E-1 for example, the density of small local defects is so high that each one may provide the nucleus for a

small damage site, and many such small sites may make up the overall damage pattern.

5.3 Surface Plasma

On most shots which cause detectable damage a spark can be seen at the damage site. When a spark is not seen on damaging shots, the damage is small and the spark may just be too weak to be detectable by an observer looking through protective goggles. In any event, we believe the spark accompanies the principal damage event (Giuliano, 1972) rather than causing it, although the large area which is seen to have been affected when the coating is fogged may be an indication of some secondary plasma effect (Boling, 1972).

5.4 Electron Avalanche

Two conditions must be satisfied to cause damage by electron avalanche (Bliss, 1970). First, the intensity must be high enough that conduction electrons gain energy from the laser radiation faster than they lose it to the lattice. Second, the laser energy density must be high enough to create a critical number of conduction electrons within the duration of the pulse. Therefore, for very short duration pulses the limiting quantity is energy density while for long pulses it is intensity. The straight line segments of the curves in Figure 25 are drawn through the data points with the appropriate pulse duration dependence to give constant energy density and constant intensity thresholds.

If this mechanism is operating for the 20-psec pulse damage, the intensity criterion is exceeded by a factor of about fifty, meaning that the electrons gain energy from the field much faster than they can transfer it to the lattice leaving many of the electrons to lose their energy to the lattice after the laser pulse has ceased. For the 20-nsec, pulses, on the other hand, the transfer of energy to the lattice proceeds essentially instantaneously on the time scale of the pulse, and the physical destruction of the coatings probably starts before the pulse is over. This basic difference in timing may have something to do with the tendency for sites damaged by Q-switched pulses to be larger than expected, that is, there may be enough energy transmitted to larger radii by electron diffusion, acoustic propagation, or some other means during the pulse that less laser intensity is required to cause damage there.

If the main effect of conduction electrons is to heat the lattice, then the stress induced by thermal expansion could damage the coatings as described in Section 5. 1. But now the amount of heating at a particular point on the mirror is proportional to the electron density there, not just the local laser energy density, so spots much smaller than 1. 3 times the Gaussian diameter are expected near threshold. This is

because the number of electrons created in an avalanche process increases exponentially with some power of the electric field (Bliss, 1970) giving an electron distribution that falls much more steeply with increasing radius than the laser intensity profile.

The dependence of threshold on beam diameter is qualitatively what is predicted by a probability formulation of electron avalanche theory (Bass and Barrett, 1972), namely that the probability for finding "lucky electrons" increases and the intensity needed to achieve a given probability for damage decreases for larger beams.

Some of the arguments in Section 5.4 are admittedly speculative. Further work is necessary to put the discussion on firmer ground.

Acknowledgments

The technical and analytical assistance of E.E. Hoell, H. Miller, R.A. Clark, and C.C. Gallagher is gratefully acknowledged.

References

Bass, M., and Barrett, H.H. (1972) 3rd ASTM Symp. Damage in Laser Materials, to be published.

Bliss, E.S. (1970) Proc. 2nd ASTM Symp. Damage in Laser Materials, NBS Spec. Publ. 341, 105; also Optoelectronics 3: 99 (1971).

Bliss, E.S., and Milan, D. (1972) AFCRL Report No. 72-0233. Available from the Defense Documentation Center, the National Technical Information Center, or the authors.

Boling, N.L. (1972) Proc. 3rd ASTM Symp. Damage in Laser Materials, to be published.

Burnham, D.C. (1970) Applied Optics 9:1482.

DeShazer, L.G., and Parks, J.H. (1971) Proc. 3rd ASTM Symp. Damage in Laser Materials, NBS Spec. Publ. 356, 124.

Giuliano, C.R. (1972) IEEE J. Quantum Electron, to be published.

Milan, D. (1971) IEEE J. Quantum Electron. QE-7:319.

Winer, I.M. (1966) Applied Optics 5:1437.